Journal of Power Sources 195 (2010) 4753–4757

Contents lists available at ScienceDirect

Journal of Power Sources

journal homepage: www.elsevier.com/locate/jpowsour

Design of an optical thermal sensor for proton exchange membrane fuel cell temperature measurement using phosphor thermometry

Kristopher Inman, Xia Wang*, Brian Sangeorzan

Department of Mechanical Engineering, Oakland University, 2200 N. Squirrel Road, Rochester, MI, United States

ARTICLE INFO

Article history:
Received 26 January 2010
Received in revised form 23 February 2010
Accepted 23 February 2010
Available online 1 March 2010

Keywords:
Temperature measurement
PEM fuel cell
Optical sensors

ABSTRACT

Internal temperatures in a proton exchange membrane (PEM) fuel cell govern the ionic conductivities of the polymer electrolyte, influence the reaction rate at the electrodes, and control the water vapor pressure inside the cell. It is vital to fully understand thermal behavior in a PEM fuel cell if performance and durability are to be optimized. The objective of this research was to design, construct, and implement thermal sensors based on the principles of the lifetime-decay method of phosphor thermometry to measure temperatures inside a PEM fuel cell. Five sensors were designed and calibrated with a maximum uncertainty of ±0.6 °C. Using these sensors, surface temperatures were measured on the cathode gas diffusion layer of a 25 cm^2 PEM fuel cell. The test results demonstrate the utility of the optical temperature sensor design and provide insight into the thermal behavior found in a PEM fuel cell.

1. Introduction

Temperature plays a significant role in proton exchange membrane (PEM) fuel cell performance, durability and reliability [1–10]. Many physical and chemical phenomena which take place inside a PEM fuel cell are affected by temperature and temperature gradients. These include the polymer membrane ionic conductivity, mass transport, and reaction rates at the electrodes. Even small variations in temperature distribution can greatly affect humidity and flooding inside a cell. Water transport inside the PEM fuel cell depends on temperature and temperature distribution due to thermal transport mechanisms such as thermo-osmosis and phase-change-induced flow (*heat pipe effect*) [11]. Furthermore, the rate of electrocatalyst degradation or degradation of the catalyst layer has also been shown to be dependent upon internal temperatures as well as local humidity [2]. Even though the thermal behavior inside a PEM fuel cell is essential to its performance and durability, it is still not yet well understood due to the technical difficulties of measuring and modeling it.

Many temperature measurement techniques have been applied to measuring in situ fuel cell temperatures. These methods include the use of thermocouples, micro-electro-mechanical systems (MEMS) sensors, and pyrometry. The methods currently proposed suffer from a variety of deficiencies such as being electrically conductive or highly invasive such that the performance is altered.

Mench et al. [12] developed a method for measuring the electrolyte temperatures in a fuel cell by placing micro-thermocouples in between two Nafion sheets. In that study, only 3 out of the 8 thermocouples embedded in the electrolyte layer actually functioned after the MEA was assembled. This method can also be considered rather intrusive as the diameter of the thermocouples is also the same diameter as the electrolyte (50 μm). Wang et al. [13] constructed a fuel cell in which the surface of the GDL could be measured using pyrometry. However this method requires significant modification to a fuel cell's bipolar plate in order to accommodate an infrared transparent window and is also subject to poor accuracy due to changes in emissivity due to water formation. He et al. [14] developed a method that used two thin film gold thermistors placed between two layers of Nafion. While this method provides adequate sensitivity, the sensors block the local transport of ions through electrolyte.

Lee et al. [15] developed a micro-sensor using MEMS technology that is placed between two MEAs and guarded by two layers of parylene. Like other thin sensors that require a material to protect the sensor itself, this method blocks the local transport of ions through the electrolyte. Basu et al. [16] developed a method that uses laser absorption spectroscopy to measure both temperature and partial pressure of water inside the flow channels of a fuel cell. While this method is minimally invasive it cannot accurately read temperatures when water is present in the flow channels. It is also incapable of point measurement and only measures an average temperature inside the flow channel itself. Wilkinson et al. [17] modified the bipolar plate of a fuel cell by embedding several micro-thermocouples into the anode and cathode bipolar plates. Due to the fragile nature of the micro-thermocouples only

* Corresponding author. Tel.: +1 248 370 2224; fax: +1 248 370 4416.
E-mail address: wang@oakland.edu (X. Wang).

0378-7753/$ – see front matter © 2010 Elsevier B.V. All rights reserved.
doi:10.1016/j.jpowsour.2010.02.071

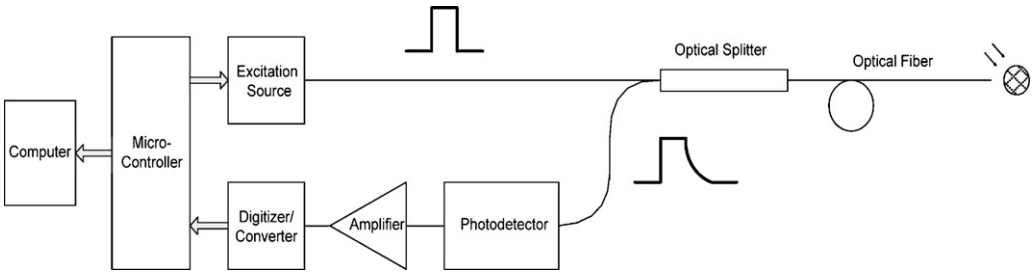

Fig. 1. Diagram of optical temperature measurement system for PEM fuel cell temperature measurement.

10 micro-thermocouples were actually operable, 9 of which were located on the anode side of the fuel cell. Additionally, the effects of changes in current distribution in the bipolar plate were not considered as this might affect the accuracy of the thermocouples due to electromagnetic interference.

Bégot and Kauffmann [18] estimated internal fuel cell temperatures using measured external endplate temperatures. They used the endplate temperatures, measured by high accuracy thermocouples, as boundary conditions to a two-dimensional fuel cell model in order to estimate internal fuel cell temperatures. While this method is unobtrusive, it provides poor accuracy of internal temperatures and yields a very slow response time due to the required thermal conductivity of the fuel cell components. David et al. [19] developed an optical method for measuring the internal temperatures of a fuel cell using Bragg fiber temperature sensors. Unlike other thermoelectric sensors, Bragg fiber sensors are immune to electromagnetic interference (EMI) and are electrically non-conductive so they require no insulation. However, the Bragg fiber sensors used are not capable of point measurement as they measure an average temperature along an approximate 1 cm length of the fiber.

There has been a considerable amount of work in the development on non-isothermal numerical models of PEM fuel cells. However, there has been very little experimental data available verifying the accuracy of these models due to the difficulty of obtaining experimental results. The purpose of this work is to design reliable and durable fiber optic sensors that can be used to determine the thermal behavior and temperature distributions inside a PEM fuel cell. The sensors will be embedded in the bipolar plate and at the surface of the gas diffusion layer to measure internal temperatures of the fuel cell at different points across the surface of the membrane electrode assembly. By using minimally invasive sensors, more realistic temperature measurements can be made under any practical operating condition. The results of the experiment should provide information of temperature distributions across the MEA along with reliable temperature data that could be used to verify PEMFC models.

2. Principles of phosphor thermometry

The principles of phosphor thermometry provide the basis for the design of the temperature sensor developed in this study. Phosphor thermometry is a well established method that possesses several qualities which make it an ideal choice for temperature measurement in a PEM fuel cell environment. Some of these qualities are electromagnetic immunity (not electrically conductive), small sensor size, and the fact that the sensors are chemically, electrically, and thermally inert even well above normal PEMFC operating temperatures [20].

The temperature measurement method for the optical sensor developed in this work is known as the "lifetime-decay method" [21] and is based on the decay mechanism of the phosphor emission. The method consists of exciting the electrons of the phosphor to a higher level with an external energy source, then observing the behavior of the emitted light when the excitation source is removed. When the excitation source is removed or deactivated, the electrons in the phosphor will, in time, return to the ground equilibrium state, thereby emitting energy that was originally absorbed from the excitation source. This emitted energy is manifested in two components: a radiation emission (light) and a non-radiative emission. The non-radiative mechanisms of the phosphor are temperature dependent. Because the components are complementary, the rate at which the excited electrons return to the ground state and emit light is indirectly dependent upon temperature. The radiative emission or light waveform emitted by the phosphor takes the form of an exponential decay which can be mathematically represented by Eq. (1) [22].

$$I = I_0 e^{-t/\tau} \quad (1)$$

where I is the intensity of the emitted light, I_0 is the intensity when the excitation source is first removed, t is time, and τ is the decay coefficient which is dependent upon the phosphor temperature.

3. Sensor design and construction

Each sensor contains a phosphor, an optical light guide, an optical splitter, an excitation source, and a photodetector. Fig. 1 shows the fundamental layout for a single optical sensor with all major components.

Chromium doped aluminum oxide (0.5% Cr:Al_2O_3), commonly known as ruby was chosen as phosphor because it is readily available, low cost, and has a thermal conductivity similar to other fuel cell components ($\sim$40 W m^{-2}). It has an adequate temperature coefficient of -12 μs K^{-1} for a temperature range of 270–520 K. Ruby also has a peak excitation band suitable for ultra-bright LEDs of approximately 550 nm and an emission peak wavelength of about 694 nm which is suitable for detection by many common photodiodes [23].

The excitation source used in this study was an ultra-bright green LED with a peak wavelength of 527 nm. A Hamamatsu S5973-01 photodiode was chosen since this photodiode has good quantum efficiency at the emission wavelength of the phosphor ($\sim$695 nm) and includes a lens specifically designed to be used with 1 mm optical fiber. It is also relatively low cost and has more than adequate response time which makes it suitable for this application.

Due to the potential high humidity in fuel cell environment, the type of optical fiber that is used is critical to proper sensor operation. Because the core material of most optical fibers is silica, which is highly hydrophilic, the fiber must be coated with a material to minimize the penetration of water from the surroundings into the fiber. Otherwise, changing levels of attenuation due to water absorption can result in hysteresis and nonrepeatability of the sensor. For this reason, a 560 μm optical fiber with an external polyamide coating was chosen. The polyamide coating reduces the amount of absorption of water into the silica fiber and therefore minimizes any hysteresis that would be caused by changes in attenuation.

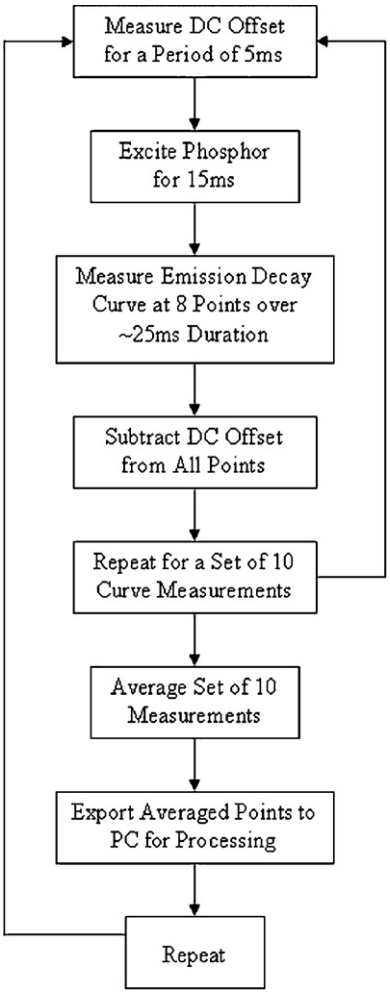

Fig. 2. Flow chart of luminescent decay measurement process used for optical temperature measurement.

4. Signal processing

Signal processing and conditioning electronics are also typically required in order to analyze the signal generated by the photodetector. A single microcontroller was connected to optical sensors to control the excitation source, perform signal conditioning and interface the sensor to a PC via USB connection. Signal data, received from the microcontroller, were averaged and sent to the PC where they were saved and available for further analysis. Obtaining a single temperature reading from each sensor is a multistep process. A flow chart showing this process is shown in Fig. 2.

This process was performed sequentially for all five temperature sensors. An example of the recorded decay signal with modified offset is shown in Fig. 3. The decay rate from all five temperature sensors is approximately the same with minor variations in decay rate. However, these variations in decay rate are not considered to be due to a difference in temperature but rather most possibly due to difference in Cr_2O_3 concentration in the ruby molecular lattice and possible impurities. Therefore, the sensors were individually calibrated.

5. Calibration of sensors

Calibration of all five optical sensors was performed by comparing temperature data from the sensors with a YSI 4600 Precision Thermometer having an accuracy of ±0.12 °C. In order to simulate the in situ conditions of a PEM fuel cell, a single gas diffusion layer was sandwiched between a graphite bipolar plate which contained the YSI resistive temperature device (RTD) sensor, and the flow channel plate of the fuel cell to be tested. This assembly was then placed in a Lindberg Blue 1100 Box Furnace where the environment of the oven was stepped in increments of approximately 10 °C from 35 to 85 °C with ramp-up and ramp-down schedules to determine if there was any influence of hysteresis. Temperature data from the YSI 4600 Thermometer and the temperature dependent decay coefficients from the optical sensors were collected during each temperature step under steady state conditions for a period of 10 min and then averaged. Decay coefficients were determined from the averaged intensity data by applying a nonlinear, least squares curve fit to Eq. (1). The decay coefficients were fit to second-order polynomials and also stored in look-up tables. Fig. 4 shows a sample of the calibration data generated from the optical sensors along with their corresponding parabolic curve fits.

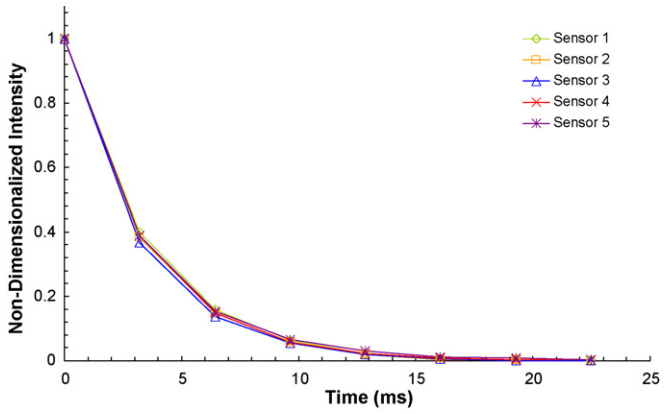

Fig. 3. Luminescent decay data sample from all five temperature sensor channels at 23 °C.

The optical sensors exhibited no measureable signs of hysteresis and had good repeatability. It should be noted that the curve-fit lines going through the data are second-order polynomials and are not linear. The magnitudes and trends of the curves agree well with results obtained by Hu et al. [24] for large sensor sizes. A linear curve fit yields a temperature coefficient of approximately 0.012 $\mu s\,K^{-1}$ which agrees with literature from Aizawa et al. [23]. Also it should be noted that theoretically, the decay coefficient should be identical for each of the five sensors. This discrepancy is considered to

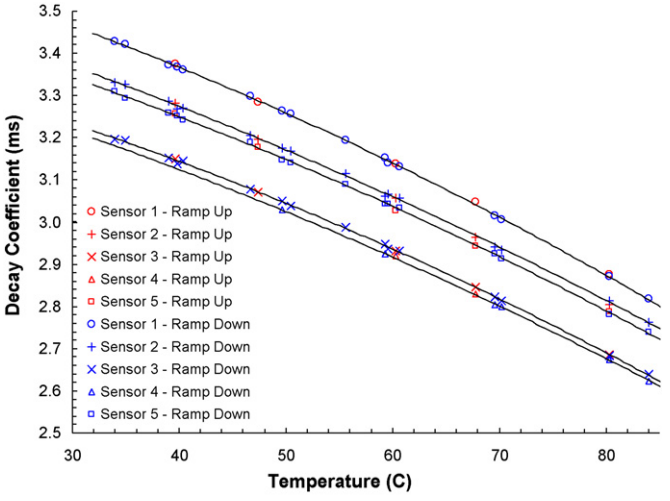

Fig. 4. Calibration results for all five optical temperature sensors from 35 °C to 85 °C.

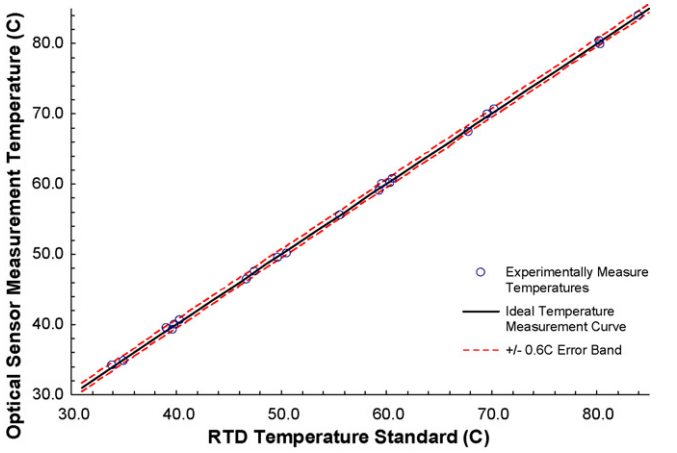

Fig. 5. Comparison between experimental optical temperature sensor measurement and YSI 4600 Precision RTD temperature standard.

be due to different chromium concentrations in each of the ruby spheres which would yield different decay coefficients at different temperatures but also yield approximately the same temperature coefficients.

After calibration, temperatures measured by the optical sensors were directly compared to that of the YSI 4600 Precision RTD to determine the success of calibration and the measurement error of each of the sensors. An example of this comparison for sensor 1 is shown in Fig. 5. The greatest temperature deviation measured among all five of the sensors was ±0.6 °C compared to RTD temperature. While greater accuracy than this is desired, it was assumed to be satisfactory for in situ in-plane fuel cell temperature measurement.

6. Experimental testing

The fuel cell used for experimental testing was a 25 cm^2 single cell PEM fuel cell. The MEA consisted of a Nafion 112 electrolyte with 0.2 mg Pt cm^{-2} and 0.4 mg Pt cm^{-2} catalyst loadings on the anode and cathode side, respectively. The flow channels plates were of a single serpentine design with 1.5 mm lands, 1 mm × 1 mm channels, and were constructed out of 8 cm × 8 cm × 0.5 cm POCO AXF-5Q graphite. Gold plated copper current collectors were used on the outside of the flow plates. The end plates were custom designed, machined in-house and constructed out of 0.5 in. thick T6061-T6 aluminum. Both anode and cathode flow plates were designed for external heaters, however only the external heater on the anode side of the fuel cell was used due to an obstructing sensor on the cathode side of the fuel cell.

The experimental fuel cell was modified in such a way that it allowed the placement of the optical sensors to be positioned normally to the surface of the cathode gas diffusion layer. To accomplish this, the optical sensors protrude through the end plate, current collector, and flow plate of the cathode side of the fuel cell. This required the fuel cell to be slightly modified by drilling 500 μm diameter holes through these three components so the optical sensors could be embedded in the cathode flow plate and make direct contact with the surface of the gas diffusion layer. As shown in Fig. 6, the five sensors were placed in such a way that they provide a maximum temperature distribution across the cell due to the flow pattern of the cathode flow plate. This involved placing sensors at the inlet, outlet, and vertically along the center of the fuel cell.

After calibration of all five optical temperature sensors, experimental testing was conducted to measure in situ temperatures inside a functioning, experimental fuel cell. The test cell was operated at different end plate temperatures, different dew point levels

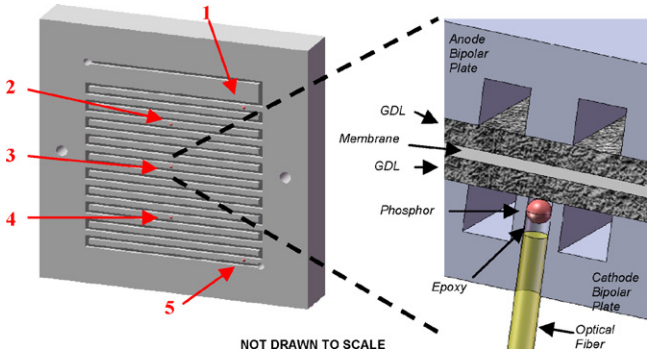

Fig. 6. Diagram of sensor placement in experimental PEM fuel cell.

and inlet temperatures in order to determine the effects humidity on local temperatures. Each test was conducted under steady state conditions, from open circuit voltage (OCV) to maximum current density while recording internal temperatures. All testing was performed using a constant stoichiometric flow rate at the anode and cathode. At each incremental test point, a time period of 10 min was allowed for the fuel cell to reach a steady state operating condition. When this steady state condition was reached, temperature data was recorded over a 10 min period and then averaged.

7. Results and discussion

The results shown in Fig. 7 were performed at a temperature of 60 °C and a dew point of 60 °C for high humidity operation. Internal temperatures are relatively sporadic with a general trend of increasing temperature as current density increases. The sporadic temperature behavior is attributed to liquid water formation inside the fuel cell combined with a low mass flow rate of air to remove that liquid water. The general trend of increasing internal temperatures with increasing current density is attributed to higher heat generation due to an increased reaction rate. It should be noted that sensors 4 and 5 have generally higher temperatures than sensors 1 through 3. This would be expected as the single serpentine flow channel design would yield greater gas temperatures at the exit of the cell due to heat addition from the electrochemical reaction on the cathode side.

In order to gain insight about the internal transient behavior of the fuel cell, results of temperature data over time was studied along for steady state conditions of fuel cell operation as shown in

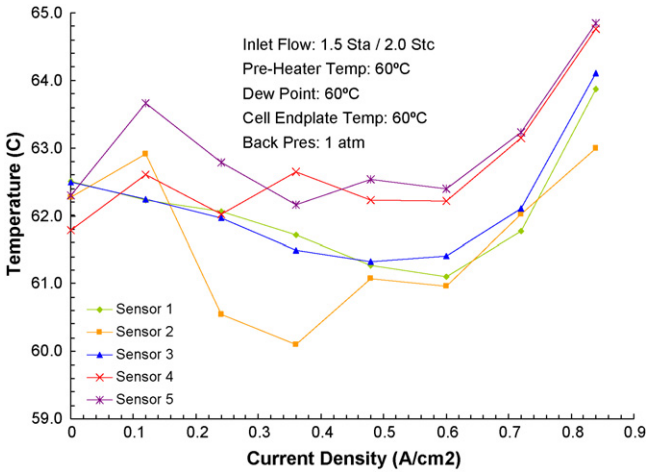

Fig. 7. Experimental PEM fuel cell in situ steady state temperature measurements with high inlet humidity.

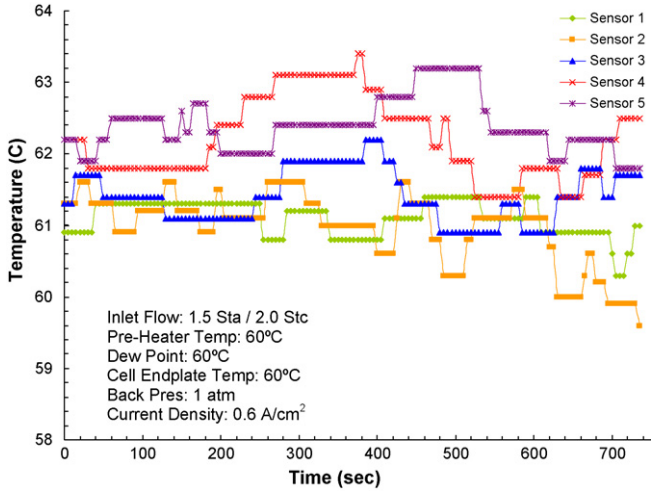

Fig. 8. Experimental PEM fuel cell in situ transient temperature measurements with high inlet humidity at 0.6 A cm^{-2} current density.

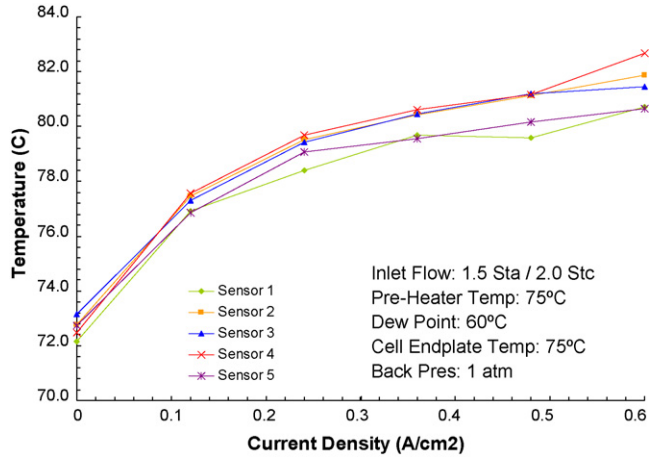

Fig. 9. Experimental PEM fuel cell in situ steady state temperature measurements with low inlet humidity.

Fig. 8. Internal fuel cell temperatures change abruptly with time and never reach a constant steady state temperature. This transient behavior is attributed to transient condensation or liquid water formation and removal in proximity of the sensors during operation.

In order to help confirm this hypothesis that water formation was the cause of temperature fluctuation, further testing was performed on the fuel cell operating at lower humidity operating conditions. Ideally, this would yield a lower presence of liquid water formation inside the fuel cell and reduce temperature fluctuation. This was done by operating the fuel cell with lower dew point temperatures on the gas inlets while maintaining pre-heater and endplate temperatures of 75 °C. The results of this testing are shown in Fig. 9. As shown in Fig. 9, operating the fuel cell at lower humidity levels yields a smaller variation in temperature between sensors, which the authors would attribute to reduced liquid water formation. The rate at which temperature increases with respect to current density is somewhat logarithmic and different from that for high humidity levels which has a more exponential trend. This difference in trends could be due to the difference in humidity and the difference in water vapor pressure between the two operating conditions. This could possibly augment the water vaporization and removal mechanisms of heat removal from the cell changing its thermal behavior with respect to a change in current density.

8. Conclusions

An optical temperature measurement method based on the principles of phosphor thermometry was entirely conceptualized, developed, and implemented in an operating PEM fuel cell. The optical temperature sensors developed were successfully calibrated within a maximum error of ±0.6 °C compared to a Precision RTD and showed no signs of hysteresis or time dependent drift. The optical sensors were able to measure in situ in-plane temperatures at the interface of the GDL and the cathode bipolar plate in a functioning, experimental fuel cell to an adequate degree of accuracy and will be a vital tool for future testing. The experimental temperature data gathered from this testing of the fuel cell provides useful information that leads to further insight into the internal thermal behavior that occurs inside of a PEMFC.

From the initial experiments conducted in this work it was found that liquid water formation has a large influence on local in situ temperatures. This was determined by measuring the temperature distribution inside a PEM fuel cell at different current densities and different operating conditions. It was also determined that heat removal by water vaporization could possible have a significant influence on the internal thermal behavior of a PEM fuel cell.

Future improvements to this method would include reducing the size and improving the placement of the phosphor. Further improvements would also be to use a phosphor with a greater temperature coefficient in order to increase the accuracy of the sensors. While ruby is sufficient for basic temperature measurement, greater accuracy might be desired for studying temperature induced mass transport phenomenon such as phase-change-induced flows.

References

[1] F. Barbir, PEM Fuel Cells: Theory and Practice, Academic Press, 2005.
[2] R.L. Borup, J.R. Davey, F.H. Garzon, D.L. Wood, M.A. Inbody, Journal of Power Sources 163 (December) (2006) 76–81.
[3] M.M. Mench, Fuel Cell Engines, Wiley, 2008.
[4] R. O'Hayre, S. Cha, W. Colella, F.B. Prinz, Fuel Cell Fundamentals, John Wiley & Sons Inc., Hoboken, NJ, 2009.
[5] J. Larminie, A. Dicks, Fuel Cell Systems Explained, Wiley, 2003.
[6] X. Li, Principles of Fuel Cells, Taylor and Francis, 2005.
[7] A. Faghri, Z. Guo, International Journal of Heat and Mass Transfer 48 (September) (2005) 3891–3920.
[8] S.G. Kandlikar, Z. Lu, Applied Thermal Engineering 29 (May) (2009) 1276–1280.
[9] C. Siegel, Energy 33 (September) (2008) 1331–1352.
[10] W. Vielstich, A. Lamm, H.A. Gasteiger, Handbook of Fuel Cells: Fundamentals, Technology, Applications, Wiley, 2003.
[11] S. Kim, M.M. Mench, Journal of The Electrochemical Society 156 (2009) B353–B362.
[12] M. Mench, D. Burford, T. Davis, Proceedings of IMECE'03, November 2003, 2003.
[13] M. Wang, H. Guo, C. Ma, Journal of Power Sources 157 (June) (2006) 181–187.
[14] S. He, M.M. Mench, S. Tadigadapa, Sensors and Actuators A: Physical 125 (January) (2006) 170–177.
[15] C. Lee, S. Lee, G. Wu, Proceedings of the 35th International MATADOR Conference, 2007, pp. 377–380.
[16] S. Basu, M. Renfro, H. Gorgun, B. Cetegen, Journal of Power Sources 159 (September) (2006) 987–994.
[17] M. Wilkinson, M. Blanco, E. Gu, J.J. Martin, D.P. Wilkinson, J.J. Zhang, H. Wang, Electrochemical and Solid-State Letters 9 (November) (2006) A507–A511.
[18] S. Bégot, J. Kauffmann, Journal of Power Sources 178 (March) (2008) 316–322.
[19] N.A. David, P.M. Wild, J. Hu, N. Djilali, Journal of Power Sources 192 (July) (2009) 376–380.
[20] Z. Zhang, L. Grattan, Fiber Optic Fluorescence Thermometry, Springer Inc., 1994.
[21] S.W. Allison, G.T. Gillies, Review of Scientific Instruments 68 (1997) 2615–2650.
[22] A.H. Khalid, K. Kontis, Sensors 8 (2008) 5673–5744.
[23] H. Aizawa, E. Toba, T. Katsumata, S. Komuro, T. Morikawa, Sensors, 2003. Proceedings of IEEE, vol. 1, 2003, pp. 88–91.
[24] Y.L. Hu, Z.Y. Zhang, K.T.V. Grattan, A.W. Palmer, B.T. Meggitt, Sensors and Actuators A: Physical 63 (October) (1997) 85–90.